Journal of Constructional Steel Research 139 (2017) 272–279

Contents lists available at ScienceDirect

Journal of Constructional Steel Research

True stress-strain curves for ASTM A992 steel for fracture simulation at elevated temperatures

Wenyu Cai [a], Mohammed A. Morovat [b], Michael D. Engelhardt [c,*]

[a] School of Civil Engineering, Hefei University of Technology, Anhui Province, China
[b] Department of Civil, Architectural and Environmental Engineering, University of Texas at Austin, USA
[c] Department of Civil, Architectural and Environmental Engineering, University of Texas at Austin, USA

ARTICLE INFO

Article history:
Received 9 March 2017
Received in revised form 27 August 2017
Accepted 20 September 2017
Available online 5 October 2017

Keywords:
ASTM A992 steel
True stress-strain curves
Elevated temperatures
Fire
Structural-fire engineering
Fracture simulations

ABSTRACT

This paper presents the results of an investigation into the development of true stress-strain curves for ASTM A992 steel at elevated temperatures up to 1000 °C. These true stress-strain curves are intended to support numerical simulations of fracture of steel members and connections subjected to heating in severe fires. Such simulations require data on true stress-strain response at very large strains associated with fracture. The true stress-strain curves developed in this study are divided into two main parts; the part prior to necking and the part after the onset of necking. Prior to necking, true stress-strain curves are directly derived from engineering stress-strain curves of ASTM A992 steel determined from high-temperature tensile coupon tests. After the onset of necking, true stress-strain curves are inferred from the engineering stress-strain curves by a trial and error process involving finite element simulations of tension coupon tests.

1. Introduction and background

In recent years, there has been increasing interest in the use of the finite element method for predicting ductile fracture of steel members and connections. Much of this work has focused on simulating fracture behavior at ambient temperature [1–3], while more recent work has also considered fracture simulations at elevated temperatures associated with severe fires [4,5]. Such simulations provide a powerful tool for researchers and designers to predict the response of steel structures to extreme loads, including fire.

Like numerical fracture predictions at room temperature, numerical fracture simulations at elevated temperatures require describing material response in terms of true stresses and strains, as opposed to the more conventional engineering stresses and strains. In addition, elevated-temperature fracture simulations require data on true stress-strain response at very large strains associated with ductile fracture.

The mechanical response of steel is conventionally represented using engineering stresses and strains. The engineering stress-strain response of steel is usually calculated using axial load and elongation measurements during a tension coupon test. Engineering stress, σ_e, is computed as the applied tension load on the coupon divided by the original cross sectional area ($\sigma_e = P/A_o$). Engineering strain, ε_e, is computed as the increase in length of the original gage length divided by the original gage length ($\varepsilon_e = \delta/L_o$).

Since the cross sectional area of the coupon varies throughout the test, the mechanical response of steel is more accurately represented using true stresses and strains, as opposed to engineering stresses and strains. A well-established concept covered in many standard texts on mechanical behavior of materials [e.g. 6,7], true stress, σ_t, is defined as the applied tension load on the coupon divided by the actual cross-sectional area (i.e. $\sigma_t = P/A$). True strain, ε_t, is defined as the sum of incremental strains, where each increment of strain is defined by the increment of deformation divided by the instantaneous gage length ($\varepsilon_t = \ln L/L_o$).

Prior to necking, a true stress-strain curve can be derived from a measured engineering stress-strain curve using Eqs. (1) and (2).

$$\varepsilon_t = \ln(1+\varepsilon_e) \tag{1}$$

$$\sigma_t = \sigma_e(1+\varepsilon_e) \tag{2}$$

As introduced before, in Eqs. (1) and (2), σ_t, ε_t, σ_e, and ε_e are true stress, true strain, engineering stress, and engineering strain, respectively. The formulas shown in Eqs. (1) and (2) are based on the assumptions of uniform stress and strain over the gage length and on the assumption of constant volume of material within the gage length [6,7]. While these assumptions are reasonable for a steel tension coupon

* Corresponding author: Ferguson Structural Engineering Laboratory, University of Texas at Austin, 10100 Burnet Road, Building 177, Austin, TX 78758, USA.
E-mail addresses: wenyucai@utexas.edu (W. Cai), morovatma@utexas.edu (M.A. Morovat), mde@mail.utexas.edu (M.D. Engelhardt).

https://doi.org/10.1016/j.jcsr.2017.09.024
0143-974X/

prior to necking, they are no longer valid after necking. The state of stress and strain is complex and highly non-uniform within the necked region. Consequently, determining the true stress-strain curve for steel from a measured engineering stress-strain curve after the onset of necking becomes difficult. However, as mentioned before, when conducting finite element simulations of steel components at or near the onset of ductile fracture, the post-necking true stress-strain curve is needed.

A number of researchers have attempted in the past to develop expressions for the post-necking true stress-strain response of metals. These include studies by Aronofsky [8], Bridgman [9], Ling [10], Zhang et al. [11], and Choung and Cho [12]. The approaches developed in these studies required assumptions about deformations within the necked zone, and in some cases, measurements of the necked zone during a tension coupon test. While these early studies provide significant insights into the factors affecting the post-necking true stress-stain curves for metals, they do not lead to a practical method for establishing these curves.

More recently, several researchers have attempted to develop post-necking true stress-strain curves for metals by conducting finite element simulations of tension coupon tests [13–15]. With this approach, a finite element model is developed for a tension coupon, with an assumed true stress-strain curve for the coupon material. The assumed true stress-strain curve is then adjusted through a trial and error procedure to develop a post-necking true stress-strain curve that results in good agreement between the engineering stress-strain curves from simulated and tested tension coupons. This approach does not require any assumptions about deformations within the necked zone, nor does it require any correction for the stress triaxiality within the necked region. As will be discussed in more detail in this paper, the authors have adopted this same approach to estimate the post-necking true stress-strain curves for ASTM A992 steel at both ambient and elevated temperatures.

In the remainder of this paper, the experimental data on ASTM A992 steel used to calibrate the true stress-strain models are first introduced. The methodology utilized to develop true stress-strain curves for ASTM A992 steel at ambient and elevated temperatures is then described. Finally, the proposed true stress-strain models are presented and some of the current limitations of the proposed models are discussed.

2. Experimental tension coupon data for ASTM A992 steel

The experimental tension coupon data for ASTM A992 steel used in this study were the test results reported by Lee et al. [16]. Lee et al. studied the mechanical properties of ASTM A992 steel at elevated temperatures up to 1000 °C by conducting steady-state temperature tensile tests. The work by Lee et al. was chosen as this was the only data found in the literature with elevated-temperature tension coupon test results for ASTM A992 steel, where the full engineering stress-strain curves up through fracture were measured and reported.

In their study, Lee et al. conducted tension coupon tests on three different samples of ASTM A992 steel taken from different production heats. The three samples were referred to as MA, MB and MC. Materials MA and MB were cut from the webs of two different W760 × 147 (W30 × 99 in U.S. Customary Units) sections, whereas material MC was cut from the flanges of a W100 × 19.3 (W4 × 13 in U.S. Customary Units) section. Fig. 1 shows the coupon dimensions as well as their orientation with respect to the rolling direction. The measured engineering stress-strain curves for these three material samples are shown in Fig. 2 for temperatures ranging from 20 °C to 1000 °C. The curves are shown at two different scales. The first shows the full stress-strain curves up through fracture. The second shows the initial portion of the stress-strain curves. All tests were conducted at a constant machine crosshead displacement rate of 0.25 mm/min.

3. Development of true stress-strain curves

In this section, the development of full range true stress-strain curves for ASTM A992 steel will be presented and discussed. The term *full range* as used herein is intended to describe true stress-strain curves that cover the full range of strains, starting at zero and extending to very large strains associated with ductile fracture. More specifically, the true stress-strain curves continue to very large strains with no specified termination. It is therefore assumed that a separate fracture-initiation criterion, implemented in the numerical simulation, indicates the termination of the true stress-strain curves. A number of such criteria are reported in the literature [13,17–20]. These criteria generally predict the equivalent plastic strain at initiation of fracture as a function of the state of stress, most notably as a function of stress triaxiality. Consequently, the true stress-strain curve is not used explicitly to predict fracture initiation, but must be accurate at the very large strains at which ductile fracture initiation occurs.

The true stress-strain curves developed in this study are divided into two main parts; the part prior to necking and the part after the onset of necking. Prior to necking, true stress-strain curves are directly derived from engineering stress-strain curves of ASTM A992 steel reported by Lee et al. [16] and shown in Fig. 2. After the onset of necking, true stress-strain curves are inferred from experimental engineering stress-strain curves by a trial and error process involving finite element simulations of tension coupon tests.

3.1. True stress-strain curves before the onset of necking

True stress-strain curves before necking consist of two main regions: the elastic region and the plastic region. The *elastic region* is defined as the region between the origin and the proportional limit, up to which stress is directly proportional to strain. Since engineering stresses and strains are very small in the elastic region, there is essentially no difference between the true and engineering stresses and strains in this region. Therefore, Eqs. (1) and (2) are utilized to obtain true stresses and true strains in the elastic region despite the fact that the assumption of volume constancy is not valid in this region. The calculated true stresses and true strains at the proportional limit for each specimen and for different temperatures are listed in Tables 1 and 2. In addition, the true stress-strain

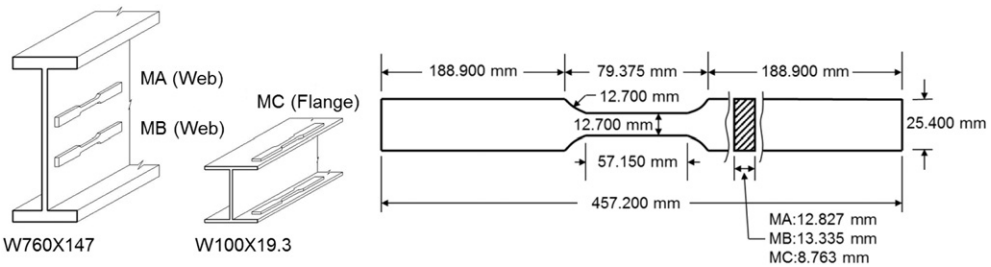

Fig. 1. Coupon specimens from tests by Lee et al. [16].

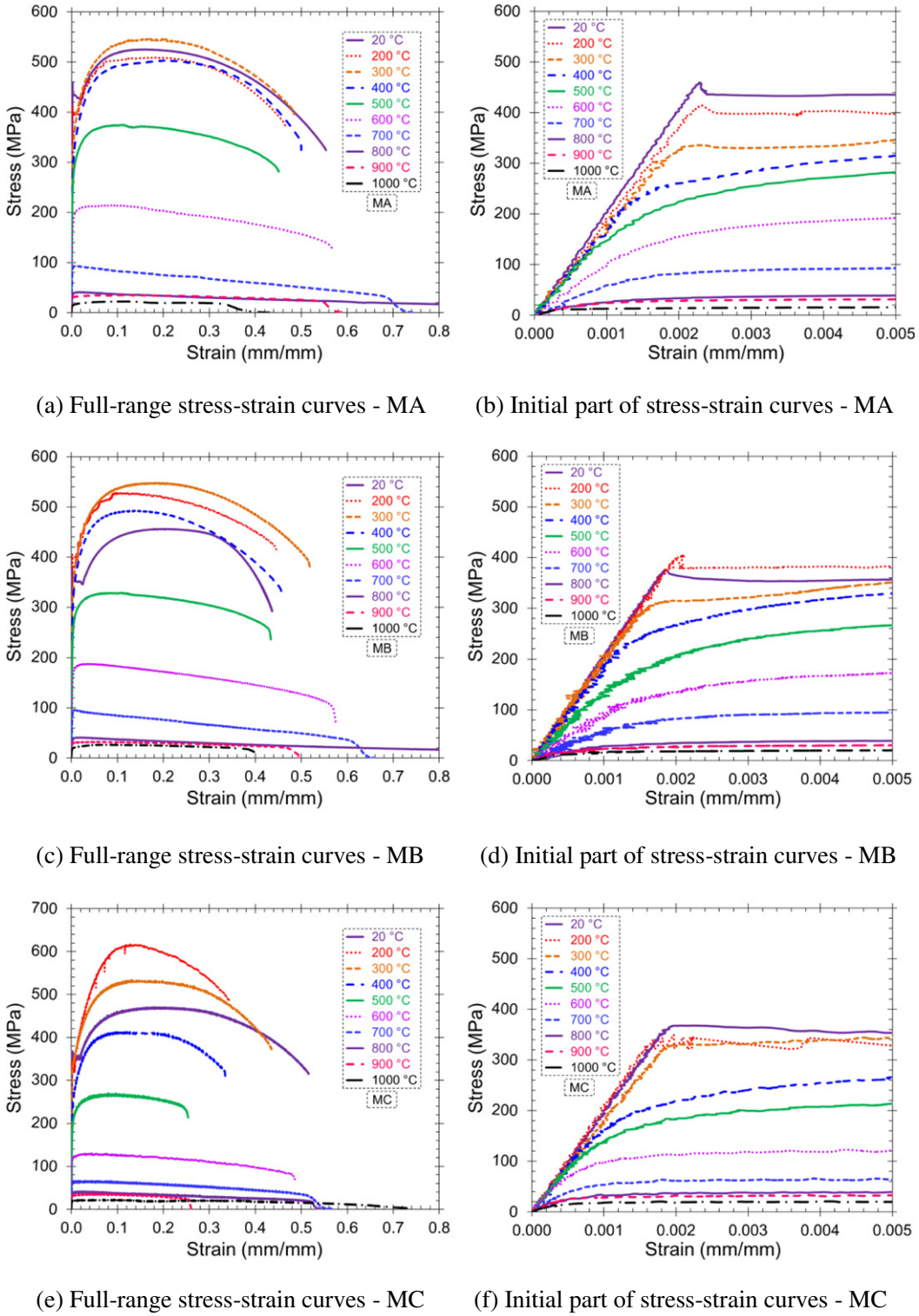

(a) Full-range stress-strain curves - MA (b) Initial part of stress-strain curves - MA

(c) Full-range stress-strain curves - MB (d) Initial part of stress-strain curves - MB

(e) Full-range stress-strain curves - MC (f) Initial part of stress-strain curves - MC

Fig. 2. Engineering stress-strain curves for ASTM A992 material samples MA, MB and MC [16].

Table 1
True stress corresponding to proportional limit (MPa).

Temperature (°C)	20	200	300	400	500	600	700	800	900	1000
MA	455	400	331	303	276	186	90	38	30	14
MB	379	379	338	317	269	165	90	38	29	24
MC	365	324	345	241	207	117	62	38	31	19
Average	400	368	338	287	251	156	80	38	30	19

Table 2
True strain corresponding to proportional limit (%).

Temperature (°C)	20	200	300	400	500	600	700	800	900	1000
MA	0.23	0.23	0.22	0.18	0.17	0.15	0.13	0.11	0.07	0.03
MB	0.19	0.21	0.18	0.15	0.30	0.11	0.13	0.09	0.07	0.03
MC	0.19	0.17	0.19	0.13	0.09	0.07	0.06	0.04	0.05	0.04
Average	0.20	0.20	0.20	0.15	0.19	0.11	0.10	0.08	0.07	0.03

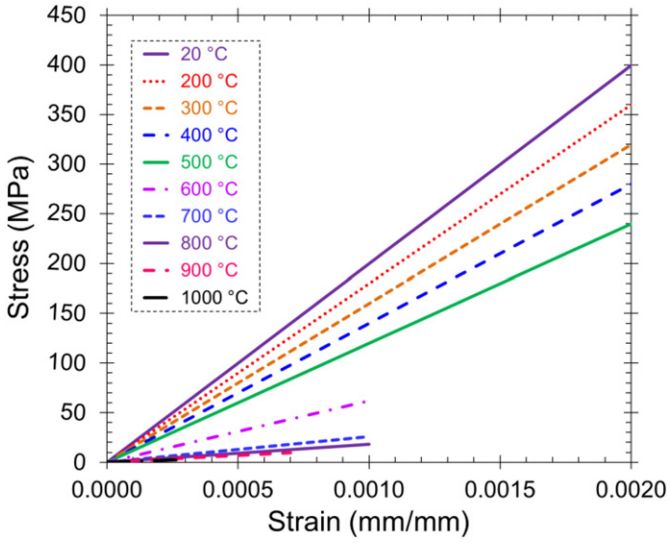

Fig. 3. True stress-strain relationship in elastic region at elevated temperatures.

relationship in the linear elastic region is plotted in Fig. 3. As seen in Tables 1 and 2, and in Fig. 3, the values of both true stresses and true strains corresponding to the proportional limit are decreasing with increasing temperatures, especially for temperatures at and above 500 °C. In other words, at higher temperatures, nonlinear material response initiates at smaller strains.

The *plastic region* is designated as the region starting from the proportional limit and ending up at the point corresponding to the onset of necking, which is taken as the point corresponding to the maximum engineering stress. In the proposed model, the plastic region consists of a yield plateau and the strain hardening region for temperatures at or below 200 °C. For temperatures equal to or greater than 300 °C, the plastic region includes the strain hardening region only. These choices are based on the observation that engineering stress-strain curves from tension experiments at 20 °C and 200 °C exhibit a yield plateau, while no apparent yield plateau can be observed in stress-strain curves for temperatures at or above 300 °C (refer to experimental results in Fig. 2).

In the plastic region, true stresses and strains were again directly calculated from engineering stresses and strains using Eqs. (1) and (2). The calculated values for true stresses and strains at the onset of necking are summarized in Tables 3 and 4 for each specimen and at different temperatures.

As indicated in previous works from literature [7,21] and further observed in this study, the relationship between true stresses and true strains in the strain-hardening region at elevated temperatures can be represented by a simple power law function shown as Eq. (3):

$$\sigma_t = K\,\varepsilon_{tp}^{n} \tag{3}$$

In Eq. (3), the temperature-dependent material parameters K and n are referred to as the strength coefficient, and the strain-hardening exponent, respectively. Calculated values for the material parameters K and n are shown in Tables 5 and 6 for various temperatures.

The values of true stress and true strain at the onset of necking are determined using Eqs. 1 and 2, as these represent the final points for which these two equations are valid. For this purpose, the onset of necking is taken to occur at the peak engineering stress, which can be determined from the engineering stress-strain curve. The engineering strain at the onset of necking can also be determined from the engineering stress-strain curve as the engineering strain corresponding to the peak engineering stress.

3.2. True stress-strain curves after the onset of necking

To develop equations for true stress-strain curves after necking, the tension coupon tests described in section 2 were simulated using the general-purpose finite element program Abaqus (Abaqus/Standard solver version 6.12) [22]. The coupons were modeled using three-dimensional solid elements. Based on an evaluation of several possible types of elements, the C3D8R element was chosen [4]. C3D8R is a three-dimensional, hexahedral eight-node linear brick element with reduced integration and hourglass control [22]. Based on limited mesh sensitivity studies, an element size of 0.10-in. was further selected to discretize the coupon models [4]. Nonlinear geometry was used in the

Table 5
Strength coefficient K (MPa).

Temperature (°C)	20	200	300	400	500	600	700	800	900	1000
MA	807	800	793	862	524	290	97	41	41	34
MB	724	724	827	758	455	214	103	48	41	34
MC	752	758	758	655	359	159	69	48	48	28
Average	761	761	793	758	446	221	90	46	44	32

Table 6
Strain-hardening exponent n.

Temperature (°C)	20	200	300	400	500	600	700	800	900	1000
MA	0.15	0.16	0.18	0.19	0.10	0.09	0.01	0.02	0.05	0.12
MB	0.16	0.13	0.15	0.13	0.10	0.03	0.01	0.02	0.05	0.06
MC	0.15	0.15	0.12	0.13	0.08	0.04	0.00	0.02	0.06	0.08
Average	0.15	0.15	0.15	0.15	0.09	0.05	0.01	0.02	0.05	0.09

Table 3
True stress at the onset of necking (MPa).

Temperature (°C)	20	200	300	400	500	600	700	800	900	1000
MA	609	598	654	611	416	234	94	41	37	26
MB	538	587	648	561	364	194	97	42	34	28
MC	556	699	603	461	292	137	66	43	38	24
Average	567	628	635	544	357	188	85	42	36	26

Table 4
True strain at the onset of necking (%).

Temperature (°C)	20	200	300	400	500	600	700	800	900	1000
MA	14.8	16.2	18.1	19.3	10.4	8.8	0.8	1.8	4.7	12.3
MB	16.5	10.6	16.7	13.0	10.1	3.2	0.8	2.2	5.1	6.2
MC	16.6	12.6	12.2	10.6	7.8	4.3	0.4	1.8	6.2	8.4
Average	16.0	13.0	16.0	14.0	9.0	5.0	1.0	2.0	5.0	9.0

Table 7
Slope of true stress-strain curves after the onset of necking (MPa).

Temperature (°C)	20	200	300	400	500	600	700	800	900	1000
MA	414	414	414	345	276	138	34	14	14	7
MB	414	414	414	345	276	138	34	14	14	7
MC	414	414	414	345	276	138	34	14	14	7
Average	414	414	414	345	276	138	34	14	14	7

Table 8
True strain at maximum true stress (%).

Temperature (°C)	20	200	300	400	500	600	700	800	900	1000
MA	55	47	48	50	45	57	74	128	59	43
MB	44	45	52	46	43	57	61	110	49	40
MC	52	34	44	33	25	49	57	54	26	74
Average	50	42	48	43	38	54	64	97	45	52

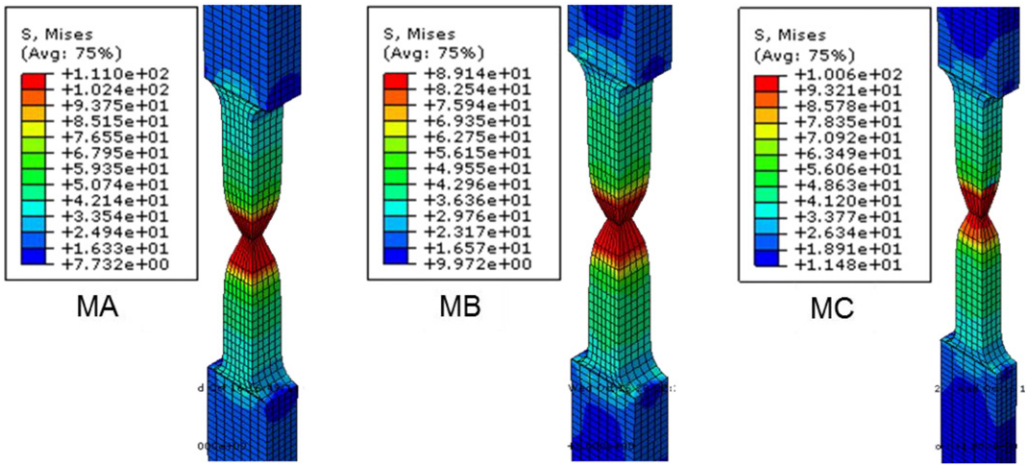

Fig. 4. Neck formation in coupon simulations at room temperature.

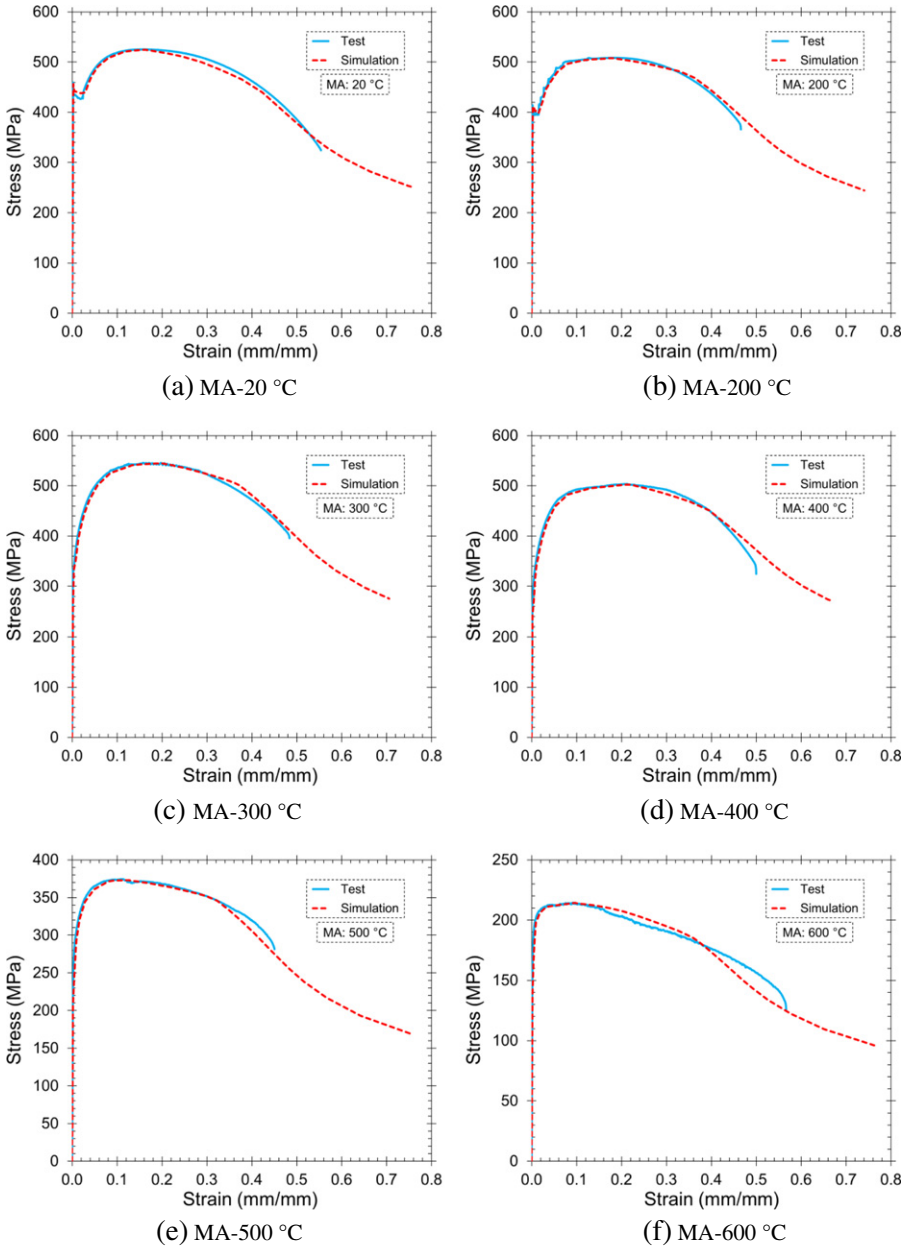

Fig. 5. Comparison of engineering stress-strain curves between tests and simulations.

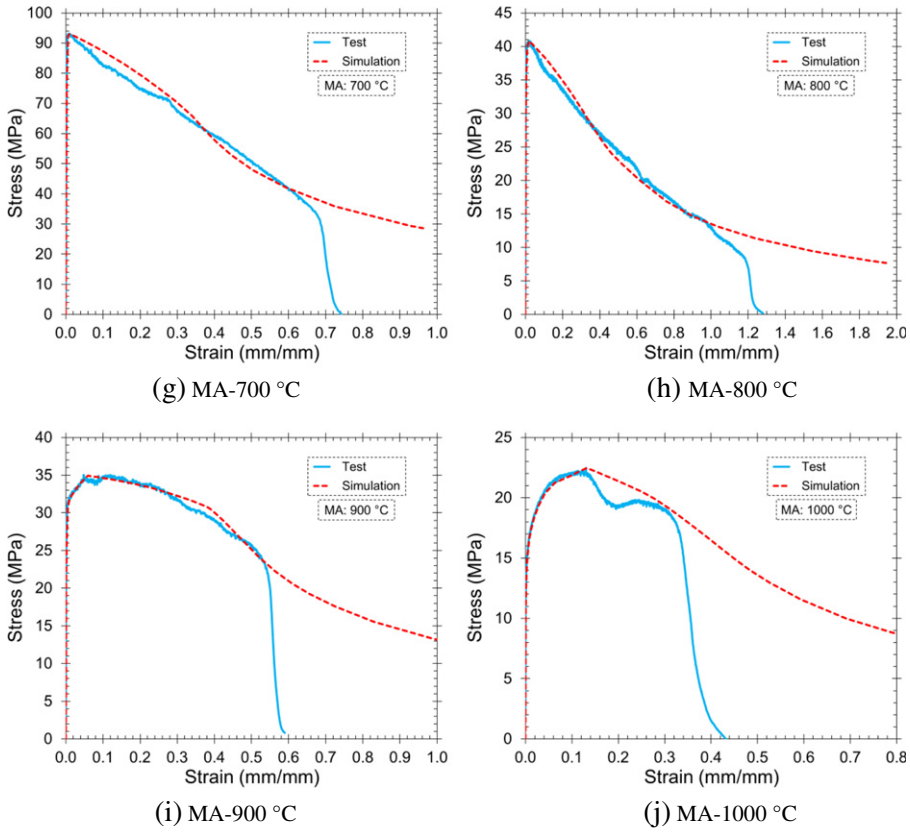

Fig. 5 (*continued*).

analysis to capture the change in coupon geometry, including necking, during the loading process. Further detailed discussions on issues related to numerical modeling techniques used in this study are provided in Cai [4].

Material properties for the Abaqus tension coupon models were input as user specified true stress-strain curves combined with the von Mises yield criterion. Prior to necking, the true stress-strain curves used in the model were derived from the measured engineering stress-strain curves (Fig. 2) using Eqs. (1) and (2), as described earlier. After necking, a trial and error process was used to establish a true stress-strain curve that resulted in a close match between the measured and simulated engineering stress-strain curves at each temperature. The true stress-strain curves beyond necking can be expressed in different ways, including multi-linear functions and power law functions. In this study, the post-necking true stress-strain response is represented using a bilinear approach, as this generated reasonably accurate results using a relatively simple procedure of calibration. The first linear segment of the proposed bilinear model has a positive slope and the second linear segment has zero slope. The calculated slopes of the first linear segment at different temperatures are listed in Table 7. For any given temperature, it was found that the slope of the true stress-strain curve after the onset of necking was remarkably similar for all three materials, and was therefore taken as a constant, as shown in Table 7. It is unclear to the writers if this consistency among the three materials for this slope was coincidence, or reflects a more fundamental aspect of material behavior. Additional experimental data is needed to further explore this issue.

By trial and error, it was also found that the point of maximum true stress (i.e. the end of first linear segment) could be located at the true strain with a value equal to engineering strain at fracture. The calculated true strains corresponding to the maximum true stresses at elevated temperatures are tabulated in Table 8.

Table 9
The proposed model for true stress-strain behavior of ASTM A992 steel at elevated temperatures.

Strain Range	True Stress (σ_t)	
$\varepsilon_t \le \varepsilon_{ty}$	$E_t\,\varepsilon_t$	(Elastic)
$0.002 \le \varepsilon_t \le 0.02$ (20 °C) $0.002 \le \varepsilon_t \le 0.01$ (200 °C)	$E_t\,\varepsilon_{ty}$	(Yield plateau)
$\varepsilon_{tsh} \le \varepsilon_t \le \varepsilon_{t\text{-}neck}$	$K\varepsilon_t^n$	(Strain-hardening)
$\varepsilon_{t\text{-}neck} \le \varepsilon_t$ and $\varepsilon_t \le \varepsilon_{tu}$	$(\varepsilon_t - \varepsilon_{t\text{-}neck})S + K\varepsilon_{t\text{-}neck}^n$	(After necking)
$\varepsilon_{t\text{-}neck} \le \varepsilon_t$ and $\varepsilon_t \ge \varepsilon_{tu}$	$(\varepsilon_{tu} - \varepsilon_{t\text{-}neck})S + K\varepsilon_{t\text{-}neck}^n$	
Definition of terms	E_t: elastic modulus ε_{ty}: true strain at proportional limit ε_{tsh}: true strain at the onset of strain-hardening $\varepsilon_{t\text{-}neck}$: true strain at the onset of necking ε_{tu}: true strain at maximum true stress S: slope of the first linear part of true stress-strain curve after the onset of necking	

Table 10
Modeling parameters for the proposed true stress-strain behavior of ASTM A992 steel at elevated temperatures.

Temperature (°C)	Elastic		Strain-hardening to necking				After necking	
	ε_{ty} (%)	E (GPa)	ε_{tsh} (%)	K (MPa)	n	$\varepsilon_{t\text{-necking}}$ (%)	Slope (S) (MPa)	ε_{tu} (%)
20	0.20	200	2.00	761	0.15	16	414	50
200	0.20	180	1.00	761	0.15	13	414	42
300	0.20	160	0.20	793	0.15	16	414	48
400	0.15	140	0.15	758	0.15	14	345	43
500	0.19	120	0.19	446	0.09	9	276	38
600	0.11	62	0.11	221	0.05	5	138	54
700	0.10	26	0.10	90	0.01	1	34	64
800	0.08	18	0.08	46	0.02	2	14	97
900	0.07	13	0.07	44	0.05	5	14	45
1000	0.03	9	0.03	32	0.09	9	7	52

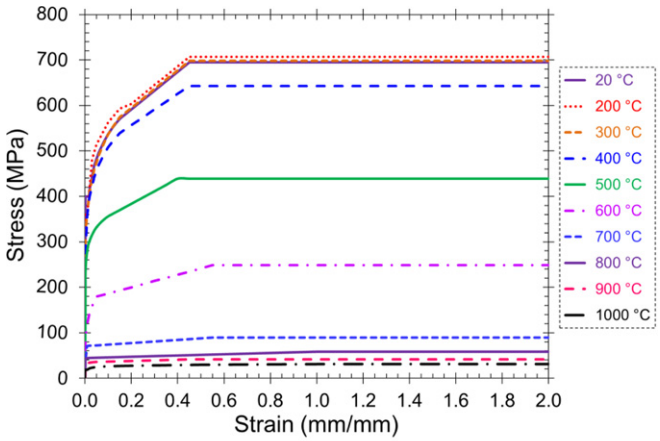

(a) Proposed true stress-strain curves plotted up to 200% true strain

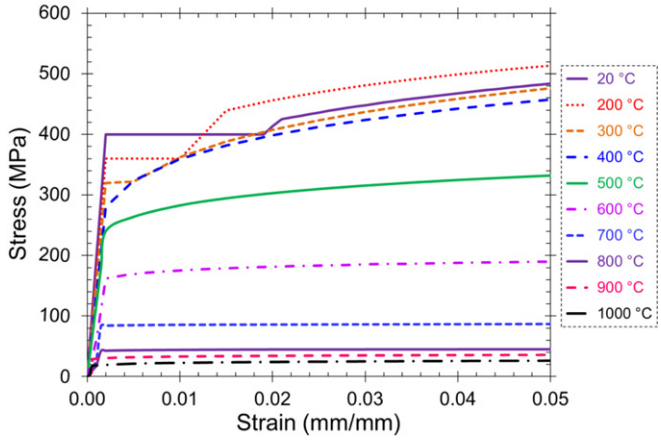

(b) Proposed true stress-strain curves plotted up to 5% true strain

Fig. 6. Proposed true stress-strain curves for ASTM A992 steel at elevated temperatures.

Note that the second linear portion of the post-necking true stress-strain curves with zero slope continues to very large strains without defining a limiting strain. In other words, since fracture is not modeled directly through the stress-strain curve, the termination of the true stress-strain curves in the proposed model does not represent fracture. Nonetheless, from experience in fracture modeling of tension coupons at elevated temperatures, it was found that maximum true strains at fracture are on the order of 150% (1.5 mm/mm) [4]. Thus, the true stress-strain curves used in fracture simulations should be defined at least up to this level of strain.

3.3. Engineering stress-strain curves – simulation versus tests

Using the techniques described above, true stress-strain curves were developed for the three material samples of ASTM A992 steel, and for temperatures ranging from 20 °C to 1000 °C. These true-stress strain curves were then used to simulate tension coupon tests on Abaqus to verify how well the experimental stress-strain curves could be predicted.

To generate engineering stress-strain curves at each temperature, axial displacements were applied to the coupon models in Abaqus to simulate the displacement-controlled tensile coupon tests conducted by Lee et al. [16]. The models simulated necking as shown in Fig. 4, but did not simulate fracture. The engineering stress-strain curves in the simulations were then computed in the same manner as in the tests. More specifically, engineering stresses were computed by taking the load on the simulated coupon and dividing by the initial cross-sectional area. Engineering strains were obtained by taking the relative displacement of two nodes along the simulated coupon that were originally 1-in. apart and then dividing by this 1-inch length. This gage distance was selected to match the gage length of the extensometer used in the tests [16].

Representative results are shown in Fig. 5 where engineering stress-strain curves from the simulations are compared with those from tests on material MA. Since fracture simulation was not included in the developed model, the engineering stress-strain curves from the simulations extend beyond the point of fracture observed in the tests. However, as illustrated in Fig. 5, the simulated curves matched the measured curves quite well up to the fracture strain level for each temperature case.

4. Proposed true stress-strain models for ASTM A992 steel

Based on the approach described in previous sections and using the averaged results of the derived true stress-strain data for materials MA, MB, and MC, a true stress-strain model for ASTM A992 Steel at elevated temperatures is proposed for steel fracture simulation. This model is illustrated in Table 9. Modeling parameters for the proposed true stress-strain model are summarized in Table 10. Note that all these model parameters are temperature dependent. Further, depending on the temperature, the proposed model for true stress-strain behavior of ASTM A992 steel at elevated temperatures consists of four or five segments, as distinct yield plateaus are absent in true stress-strain curves for temperatures at or above 300 °C.

The derived true stress-strain curves at both ambient and elevated temperatures are plotted in Fig. 6. As shown in Fig. 6(a), the true stress-strain curves are extended to very large strains, which is required for fracture simulations. Note that the curves in Fig. 6(a) are arbitrarily terminated at the true strain of about 200%. As previously discussed, the end in the true stress-strain curve is not intended to represent the initiation of fracture, and the curves in Fig. 6(a) continue indefinitely in the input to Abaqus. Fig. 6(a) further shows the bilinear model utilized to represent the true stress-strain behavior of ASTM A992 steel after the onset of necking. The initial portion of the true stress-strain curves up to 5% strain are further depicted in Fig. 6(b). Fig. 6(b) clearly shows the ability of the proposed model to consider the effect of temperature on stiffness, strength, and fundamental shape of stress-strain curves of ASTM A992 steel when exposed to fire.

5. Conclusions

This paper has described recent research on the development of true stress-strain curves for ASTM A992 steel at elevated temperatures up to 1000 °C. Using the experimental data for ASTM A992 steel together with the finite element analysis method, true stress-strain curves from the origin and extending to very large strain values were obtained. The true stress-strain curves derived in this study describe the behavior both before and after necking. A generalized function to represent the relationship between true stresses and strains after necking is proposed for use in finite element models that are intended for fracture simulations at elevated temperatures.

While the research described herein is preliminary in nature and limited in scope, it has demonstrated the potential for reasonable computational simulation for the post-necking response of tensile test coupons at elevated temperatures. Further research is needed to validate and improve the accuracy of the proposed true stress-strain curves at elevated temperatures. Specifically, the simulated tension coupon tests used to calibrate the post-necking true stress-strain response are affected by modeling techniques including mesh density, element type, model geometry, etc. The influence of these finite element modeling issues on the derived true stress-strain curves deserves further study. Additional work is also needed to assess the effect of strain rate, loading rate and load duration, as well as material variability on

the true stress-true strain response. More experimental data are also needed to verify applicability of the proposed model for intermediate temperatures.

Acknowledgments

The research reported herein was conducted as part of a research project on *Creep Buckling of Steel Columns Subjected to Fire* supported by the National Science Foundation (NSF Award 0927819). The support of the National Science Foundation and of the former NSF Program Director M.P. Singh is gratefully acknowledged.

References

[1] A.M. Kanvinde, G.G. Deierlein, Cyclic void growth model to assess ductile fracture initiation in structural steels due to ultra-low cycle fatigue, J. Eng. Mech. ASCE 133 (6) (2007) 701–712.
[2] R. Kiran, K. Khandelwal, A micromechanical model for ductile fracture prediction in ASTM A992 steel, Eng. Fract. Mech. 102 (2013) 101–117.
[3] C.M. Smith, G.G. Deierlein, A.M. Kanvinde, A Stress Weighted Damage Model for Ductile Fracture Initiation in Structural Steel Under Cyclic Loading and Generalized Stress States, The John A. Blume Earthquake Engineering Center, Department of Civil and Environmental Engineering, Stanford University, Stanford, CA, 2014 Report No. 187.
[4] W. Cai, Steel Fracture Modeling at Elevated Temperature for Structural-fire Engineering Analysis(Ph.D. Thesis), Department of Civil, Architectural, and Environmental Engineering, University of Texas at Austin, Austin, TX, 2015.
[5] W. Cai, M.D. Engelhardt, Modeling fracture of steel at elevated temperature, Proceedings of the 5th International Workshop on Performance, Protection, and Strengthening of Structures Under Extreme Loading, East Lansing, USA, 2015 250–257.
[6] D.R. Askeland, P.P. Phulé, The Science and Engineering of Materials, Brooks/Cole–Thomson Learning, 2003.
[7] G.E. Dieter, Mechanical Metallurgy, McGraw-Hill, New York-London, 1986.
[8] J. Aronofsky, Evaluation of stress distribution in the symmetrical neck of flat tensile bars, J. Appl. Mech. 18 (1) (1951) 75–84.
[9] P.W. Bridgman, Studies in Large Plastic Flow and Fracture: With Special Emphasis on the Effects of Hydrostatic Pressure, McGraw-Hill, New York-London, 1952.
[10] Y. Ling, Uniaxial true stress-strain after necking, AMP J. Technol. 5 (1996) 37–48.
[11] Z.L. Zhang, M. Hauge, J. Ødegård, C. Thaulow, Determining material true stress–strain curve from tensile specimens with rectangular cross-section, Int. J. Solids Struct. 36 (23) (1999) 3497–3516.
[12] J.M. Choung, S.R. Cho, Study on true stress correction from tensile tests, J. Mech. Sci. Technol. 22 (6) (2008) 1039–1051.
[13] Y. Bao, T. Wierzbicki, A comparative study on various ductile crack formation criteria, J. Eng. Mater. Technol. ASME 126 (3) (2004) 314–324.
[14] P. Arasaratnam, K.S. Sivakumaran, M.J. Tait, True stress-true strain models for structural steel elements, ISRN Civil Engineering 2011 (2011) Article ID 656401 https://doi.org/10.5402/2011/656401.
[15] N. Tardif, S. Kyriakides, Determination of anisotropy and material hardening for aluminum sheet metal, Int. J. Solids Struct. 49 (25) (1999) 3496–3506.
[16] J. Lee, M.A. Morovat, G. Hu, M.D. Engelhardt, E.M. Taleff, Experimental investigation of mechanical properties of ASTM A992 steel at elevated temperatures, AISC Eng. J. 50 (4) (2013) 249–272.
[17] G.R. Johnson, W.H. Cook, Fracture characteristics of three metals subjected to various strains, strain rates, temperatures and pressures, Eng. Fract. Mech. 21 (1) (1985) 31–48.
[18] J.W. Hancock, A.C. Mackenzie, On the mechanisms of ductile failure in high-strength steels subjected to multi-axial stress-states, J. Mech. Phys. Solids 24 (2–3) (1976) 147–169.
[19] H. Hooputra, H. Gese, H. Dell, H. Werner, A comprehensive failure model for crash-worthiness simulation of aluminum extrusions, Int. J. Crashworthiness 9 (5) (2004) 449–463.
[20] T. Borrvall, T. Johansson, M. Schill, J. Jergéus, K. Mattiasson, P. DuBois, A general damage initiation and evolution model (DIEM) in LS-DYNA, 9th European LS-DYNA Conference, Jun. 2–4, Manchester, UK, 2013.
[21] M.A. Morovat, Creep Buckling Behavior of Steel Columns Subjected to Fire(Ph.D. Thesis), Department of Civil, Architectural, and Environmental Engineering, University of Texas at Austin, Austin, TX, 2014.
[22] Abaqus/Standard Version 6.12, User's ManualProvidence, RI 2012.